Extended Abstract, 24th Conf. on Severe Local Storms
Amer. Meteor. Soc., Savannah, Georgia, October 26-31, 2008

17B.4 IMPROVEMENTS IN THE TREATMENT OF EVAPORATION AND MELTING IN MULTI-MOMENT VERSUS SINGLE-MOMENT BULK MICROPHYSICS: RESULTS FROM NUMERICAL SIMULATIONS OF THE 3 MAY 1999 OKLAHOMA TORNADIC STORMS

Daniel T. Dawson II*[1], Ming Xue[1], Jason A. Milbrandt[2]

[1]Center for the Analysis and Prediction of Storms and School of Meteorology
University of Oklahoma, Norman, OK 73072

[2]Numerical Weather Prediction Research Section, Environment Canada, Dorval, Québec, Canada

1. INTRODUCTION AND MOTIVATION

One of the long-standing challenges in successful numerical simulation and prediction of supercell thunderstorms has been the parameterization of cloud and precipitation microphysics. In several recent studies (Gilmore et al. 2004, van den Heever and Cotton 2004, Cohen and McCaul 2006, Snook and Xue 2006), extreme sensitivity to prescribed fixed parameters of single-moment (SM) bulk microphysics parameterizations (BMP) was found for such features as the amount of accumulated precipitation, cold pool size and strength, storm track and longevity, and even (in Snook and Xue 2006) the presence or absence of tornado-like vorticies. In addition, Markowski et al. (2002) notes that most simulations of supercells in the literature have produced cold pools that are unrealistically strong, and that, furthermore, observations of tornadic versus non-tornadic supercells indicate that tornadic supercells are characterized by warm RFD's relative to a preponderance of cold RFD's in non-tornadic storms.

In light of this well-documented sensitivity, and the significant implications for successful numerical simulation of supercells and attendant circulations, the question naturally arises as to whether this sensitivity can be alleviated or removed altogether, through improving the parameterization of microphysical processes. In the aforementioned studies, one of the parameters in the assumed particle size distribution (PSD) must be fixed or diagnosed as a function of the other parameters, since only one moment of the distribution is predicted. Typically this is the intercept parameter N_0 for the exponential distribution. Multi-moment (MM) schemes allow for more than one parameter in the PSD to vary independently of the others. For example, in a double-moment (DM) microphysics scheme that specifies exponential distributions for a given hydrometeor category, the intercept parameter N_0 is allowed to vary independently of the slope parameter λ. Multi-moment schemes have become increasingly popular in recent years (e.g., Ziegler 1985, Ferrier et al. 1995, Meyers et al. 1997, Reisner et al. 1998, Cohard and Printy 2000, Milbrandt and Yau 2005, Seifert and Beheng 2006), at least in part because of this removal of the need to specify a priori the values of one or more PSD parameters, and also due to the ever-increasing computational resources available to researchers. In addition, observational studies (e.g, Waldvogel 1974) have shown that N_0 can vary significantly in time and space within even a single convective system.

In a previous study (Dawson et al. 2007, hereafter DXMYZ2007), we reported on the results of numerical experiments designed to test the impact of single and multi-moment BMPs on high-resolution convection-resolving simulations of the 3 May 1999 Oklahoma tornado outbreak using the Advanced Regional Prediction System (ARPS, Xue et al. 2001, 2003) model. This outbreak was characterized by severe, long-lived supercells that often tracked in close proximity (within a few storm diameters) to each other without significant destructive interference, and displayed relatively weak and localized cold pools (see Fig. 1).

The first scheme used in the idealized simulations was the Lin-Tao (Lin et al. 1983, with modifications by , Tao and Simpson 1993) hereafter LIN--SM BMP, the default in ARPS. The other was the MM BMP of Milbrandt and Yau (Milbrandt and Yau 2005a, b, hereafter MY05a,b).

In DXMYZ2007, both real-data and idealized single-sounding simulations indicated better agreement with the observed reflectivity and cold-pool structures of the storms when using a multi-moment BMP, particularly in the relatively high-resolution (500-m grid-spacing and smaller) idealized simulations (see Fig. 2). In particular, the MM runs showed much weaker and smaller cold pools, in better agreement with observations (Markowski 2002), than the SM runs when typical specified values of the intercept parameter N_0 was used.

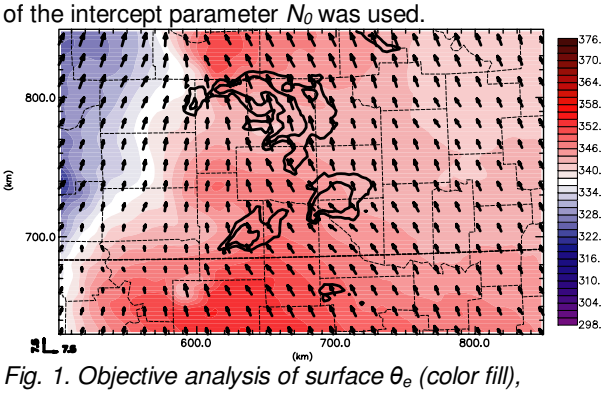

Fig. 1. Objective analysis of surface θ_e (color fill), observed reflectivity (black contours, 20 dbZ increment), and horizontal wind vectors (every 15 km, scale in m s^{-1} indicated in lower left of figure), at 0000 UTC 4 May 1999 centered over central OK.

* *Corresponding author address:* Daniel T. Dawson II, CAPS/SoM, National Weather Center, Suite 5900,120 David Boren Blvd, Norman OK 73072, USA
ddawson@ou.edu

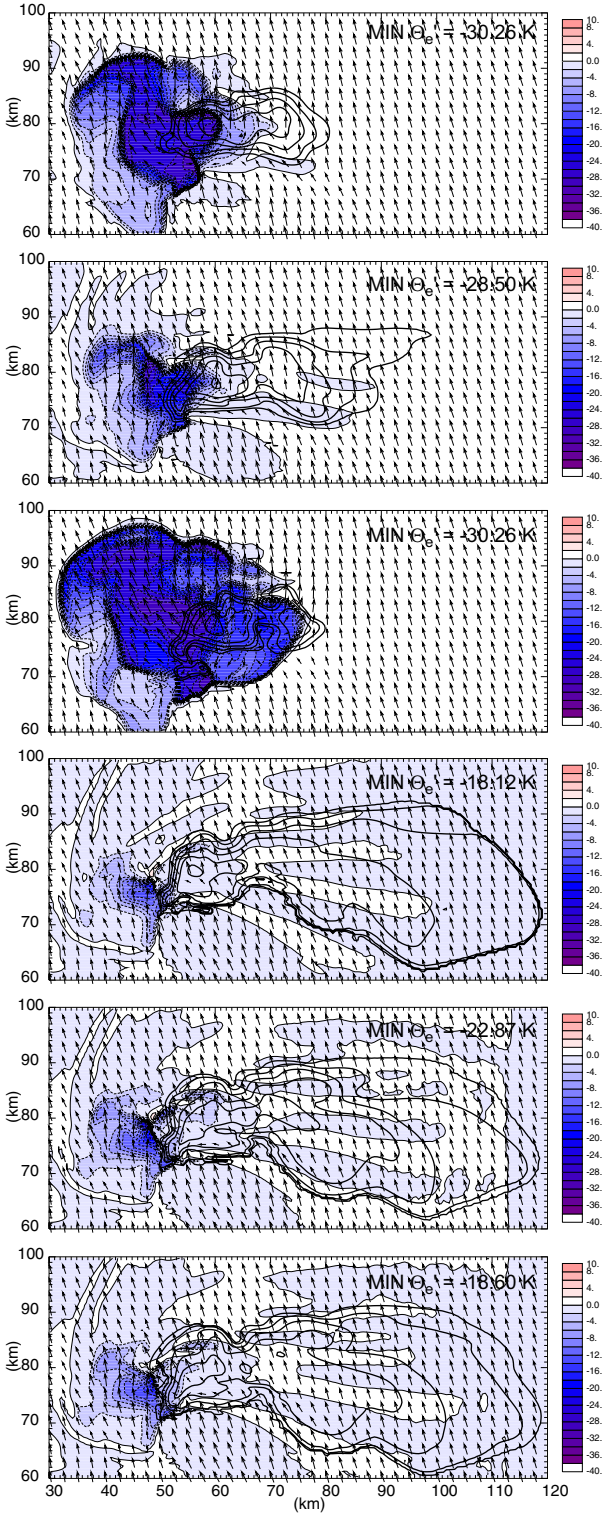

Fig. 2. Surface θ_e' (color fill), reflectivity (black contours, 20 dbZ increment), and wind vectors every 2.5 km (1 unit length = 15 m s^{-1}) at 3600 s for a) 500mLIN, b) 500mLINRN0R, c) 500mMY1, d) 500mMY2, e) 500mMY2da, f) 500mMY3.

In the current study, we examine the behavior of the simulated storms in these simulations in more detail, primarily through a detailed budget analysis of the microphysics-related thermodynamic terms in the downdrafts of the storms. Our methodology is similar to that employed by Straka and Anderson (1993) in their study of simulated microburst-producing convective storms. We integrate a form of the thermodynamic energy equation over the downdraft region, in which the effects of sublimation/deposition, melting/freezing, and evaporation/condensation are explicitly partitioned for each hydrometeor category.

In addition to the budget analysis, we analyze the behavior of selected trajectories that pass through the RFD and FFD of the storms, respectively. We analyze integrated water vapor specific humidity and potential temperature along the trajectories, with the goal of identifying the relative importance of the two main diabatic source terms: microphysical processes and turbulent mixing, for each of the simulations.

Finally, we offer physical explanations for the superior performance of the multi-moment configurations of the MY scheme in these simulations.

In particular, we find that the size-sorting process, which is modeled in the multi-moment schemes, but not in the single-moment schemes, plays a significant role within the downdraft region of the simulated storms, in general yielding a preponderance of large mean particle sizes (mainly raindrops and hailstones) at low-levels, reducing the evaporation and melting rates over those found in a single-moment treatment. In addition, the flexibility gained from allowing the total number concentration N_t of hydrometeors to vary independently of the mixing ratio q in the multi-moment scheme allows for more physically-realistic treatment of the effect of the evaporation and melting processes on changes in the distribution.

These and other effects, and general implications for high-resolution thunderstorm modeling using the multi-moment BMP approach are discussed.

Preliminary results from a new set of real-data numerical simulations, nested down to sub-1km grid spacings, of the 3 May 1999 outbreak are presented. These experiments are designed to test the results of the previous idealized simulations in the more complicated real-data prediction framework, and to assess the potential for the multi-moment microphysics approach to improve the prediction of severe thunderstorms and associated circulations, such as mesocyclones and tornadoes.

2. OVERVIEW OF SIMULATIONS

In DXMYZ2007, a set of high-resolution idealized simulations were performed using a sounding extracted from an earlier real-data simulation. We will focus on the simulations using 500-m grid-spacing in the horizontal. Three of the simulations used SM schemes, while three used MM schemes. Of the SM simulations, two used the LIN scheme with two different values of

the intercept parameter for rain N_{0x}: 8.0 x 10^6 m^{-4} and 4.0 x 10^5 m^{-4} respectively. These values are reflective of a PSD skewed toward smaller and larger drop diameters, for a given mixing ratio, respectively. The former value is equal to that in the commonly-used Marshall-Palmer (M-P) distribution (Marshall and Palmer 1948). These schemes are hereafter referred to as *500mLIN* and *500mLINRN0R*, respectively. The third SM simulation (*500mMY1*) used the single-moment mode of the MY scheme, with all PSD parameter values for precipitating hydrometeors set to the same as 500mLIN.

The MM simulations used the 2- and 3-moment versions of the MY scheme, as well as a 2-moment version where the shape parameter α is diagnosed from the mean-mass diameter, based on experiments with pure sedimentation (MY2005a). These are referred to as *500mMY2*, *500mMY2da*, and *500mMY3*. All simulations were identical except for the choice of the BMP. Convection was initiated with an ellipsoidal thermal bubble of maximum potential temperature perturbation of 4 K with a horizontal radius of 10 km and vertical radius of 1.5 km, centered 1.5 km above ground, and 35 and 25 km from the left and south edge of the domain, respectively. The dimensions of the domain were 128x175x20 km^3, and the simulations were ran out to 2 h. The reader is referred to DXMYZ2007 for further details on the configuration of the simulations.

3. MICROPHYSICS BUDGET ANALYSIS

Greater understanding of the differences in the roles of the various microphysical processes within the low-level downdraft between the various simulations can be obtained by examining a detailed budget analysis of the relevant microphysical source terms for temperature changes. At a given point, the time rate of change of temperature due to phase changes of water can be written simply as $(\partial T / \partial t)\big|_{mp} = S_{mp}$,where the subscript *mp* denotes microphysical phase changes, and S_{mp} is all source and sink terms involving phase changes of water. These are evaporation and condensation of cloud water; evaporation of rain; melting and freezing of ice crystals, snow, graupel, and hail; and collection (freezing) of cloud and rain by each of the above ice categories. Most of the processes are common to each of the schemes used in this study. However, since the LIN scheme does not contain a separate graupel category, those processes are not active in that scheme. In addition, neither the LIN nor MY scheme allows for condensation of vapor onto rain.

To determine the most important processes and how they differ among the simulations, the instantaneous rates of these processes were output at 30-s intervals for each of the simulations for two 30-min intervals into the model simulation: 1800-3600 s, and 3600-5400 s. For each 30-s time step, the temperature equation was integrated forward for each process using the instantaneous rate information at the beginning of each step. Bulk values of cooling and heating in the low-level downdraft were obtained by summing the total thermal energy change for each process, given per unit mass by $C_p \Delta T$, over all grid boxes at each time where vertical velocity w < -0.5 m s^{-1} and height z (AGL) < 4 km. Other criteria for the downdraft region may be chosen and may accordingly change the relative magnitudes of the different terms in the budget analysis, thus the results must be interpreted carefully.

The results of the budget analysis are shown in graph form for the 500-m simulations in Fig. 3, in the form of total heating/cooling for each process over the whole downdraft volume over the entire 1800-s in units of gigajoules (GJ). In general, the MM simulations are very similar in magnitude of total cooling, while the SM simulations differ from each other and the MM simulations. *500mMY1* shows less total cooling from 3600 s to 5400 s, likely because the storm was dissipating during this time period (in all other simulations the storm persists through 7200 s). Qualitatively speaking, the relative magnitudes of cooling between the various simulations are remarkably constant between the two budget time windows. The difference in total downdraft cooling between *500mLIN* and the *500mRN0R* run is significant and directly attributable to the smaller fixed N_{0r} value used in *500mRN0R*, which has a first-order effect on decreasing the rain evaporation rate. Of all the runs, *500mMY1* has the greatest magnitude of cooling, including that due to evaporation of rain. Even though the same intercept parameters were used in *500mMY1* and *500mLIN* for all precipitating species, other differences in the schemes, such as in the treatment of the cloud category and the fall speed relation for the rain category are possible reasons for the differences.

The reason for the large differences between the MM runs and the SM runs is less clear, since N_{0x} is allowed to vary in time and space for a given species *x*. Vertical profiles of horizontally and time-averaged values (using the same criteria as in the budget analysis for the downdraft region) of mixing ratio, number concentration, mean-mass diameter, and shape parameter for rain (Fig. 4) and hail (Fig. 5) were computed for the 500-m runs. Only points with non-zero hydrometeor content were included in the averaging. These plots suggest that two main differences between the MM and SM runs contribute to the smaller magnitudes of cooling in the low-level downdrafts: 1) the generally smaller mass contents of rain and hail in the downdraft, and 2) the overall larger mean-mass diameters of the particles in the MM runs. Indeed, average number concentrations of both rain and hail are 2-4 orders of magnitude smaller in the MM runs than in the SM runs, while the mixing ratios are only a factor of 2 or less smaller. This is reflected in the D_m profiles, which indicate significantly larger average particle diameters in the MM over most of the depth of the low-level downdraft as a result of size-sorting in the MM schemes.

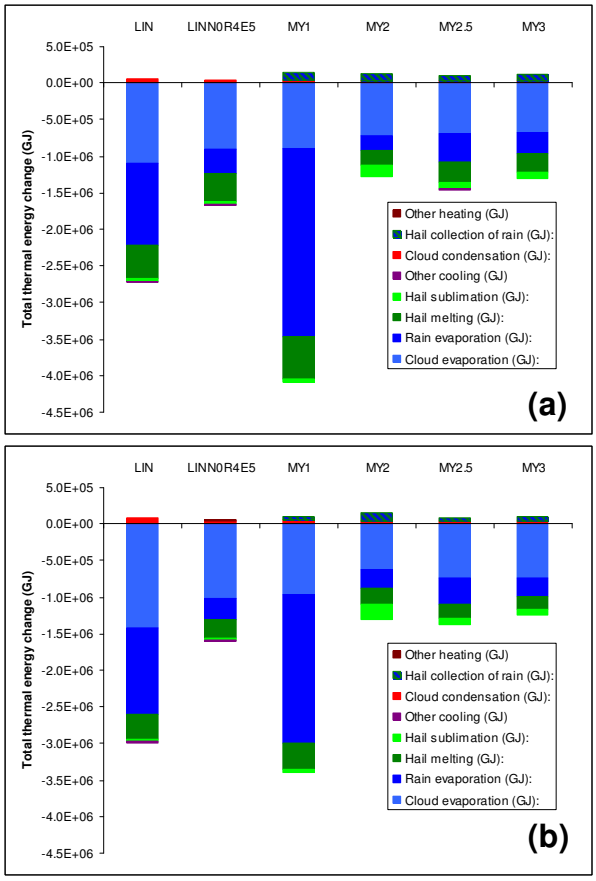

Fig. 3. Bulk thermal energy change ($c_p\Delta T$) *from microphysical processes in the low-level downdraft (defined as all grid boxes below 4 km AGL with* w *< 0.5 m* s^{-1}*) between a) 1800 s and 3600 s and b) 3600 s and 5400 s for each of the 500-m simulations.*

4. TRAJECTORY ANALYSIS

To further investigate the development of the surface cold pool within these simulations, trajectory analyses are performed. We examine trajectories terminating just above the surface in the cold pool. We examine groups of trajectories that terminate near the minimum θ_e at the surface after 45 min of simulation time for each run (see Fig. 6). The early time is chosen to minimize nonlinear differences in the development of the broad features of each storm, when comparing the trajectories. For each group of trajectories, averaging is performed at each point in time along the trajectories to yield a single "average" trajectory. Integration of the Lagrangian form of the potential temperature equation and water vapor conservation equation is also performed, in which the only source terms are turbulent+computational mixing, and microphysical processes. For this study, we use the definition of θ_e found in Bolton (1980). In principle, assuming conservation of θ_e, the source region for air entering the surface cold pool via the convective downdrafts can be

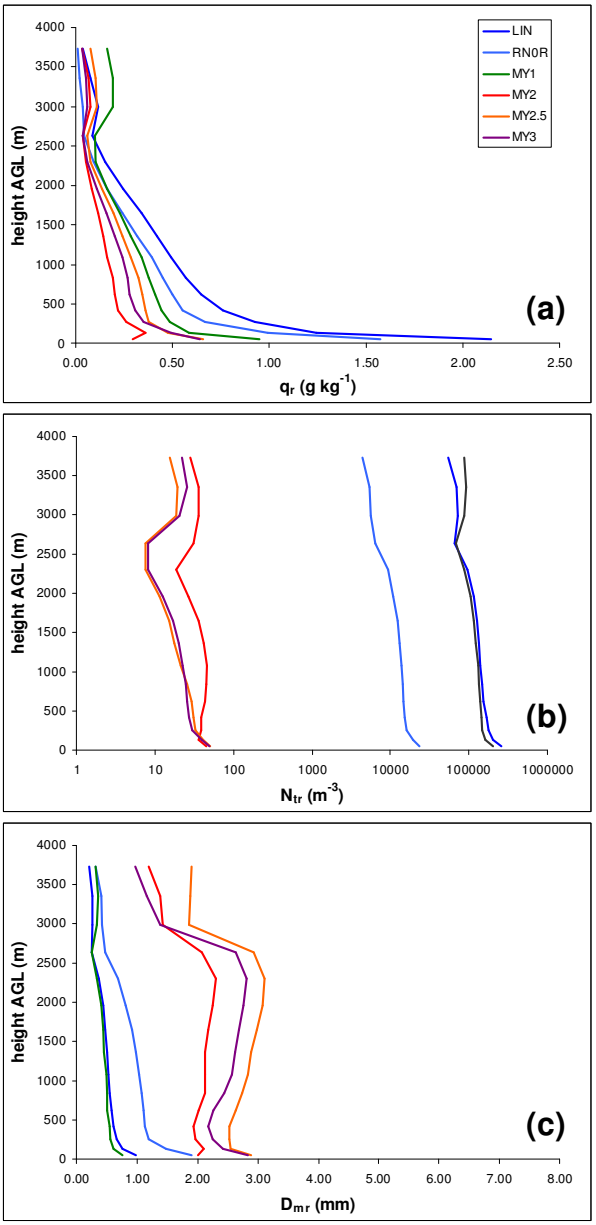

Fig. 4. Vertical profiles of horizontally and time-averaged rain PSD parameters in the low-level downdrafts of the 500-m simulations: a) mixing ratio q_r*, b) total number concentration* N_{tr}*, and c) mean-mass diameter* D_{mr}

determined by comparing with the vertical profile of θ_e in the environmental sounding.

Fig. 7 shows the average height vs. time for the trajectory group terminating near the minimum surface θ_e, along with the envelope of heights spanned by the group of trajectories at each time, for each of the simulations. Fig. 8 shows time-series of instantaneous microphysics process rates, while Fig. 9 shows the average θ_e interpolated directly to the trajectory, along with the integrated θ_e from turbulent mixing alone,

microphysical processes alone, and the two combined (θ_e is not integrated directly, but rather θ and q_v are integrated separately, from which θ_e is calculated). In principle, the total "integrated" θ_e should match that interpolated directly from the model fields, but in practice this is difficult to achieve due to errors from spatial and temporal interpolation, and due to model error (particularly advection error).

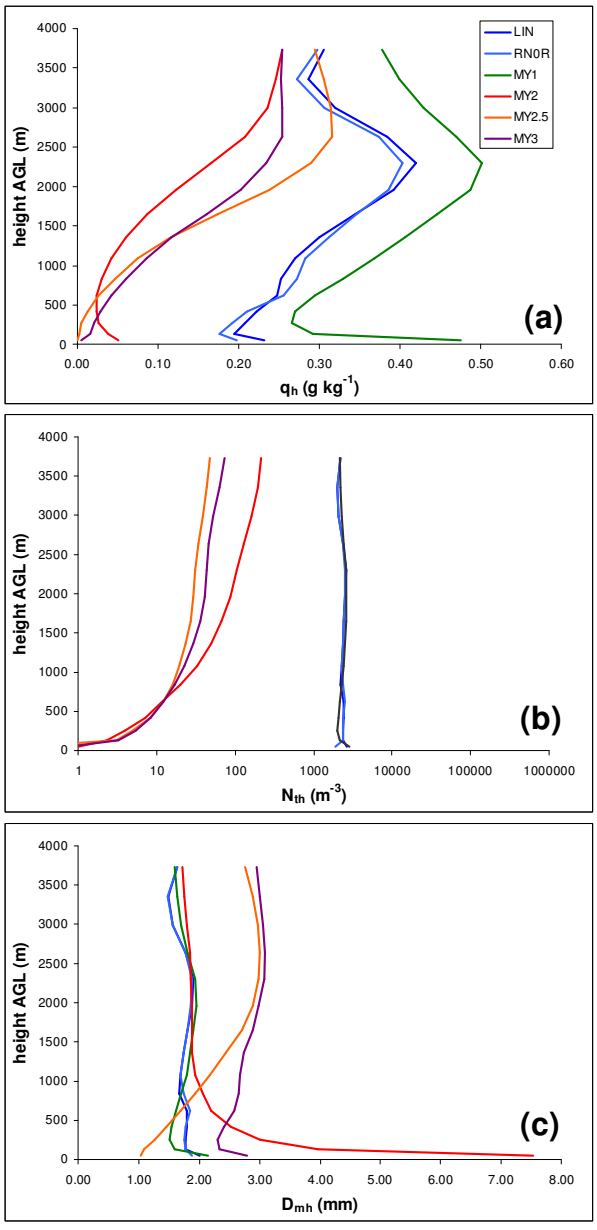

Fig. 5. As in Fig. 4 but for hail.

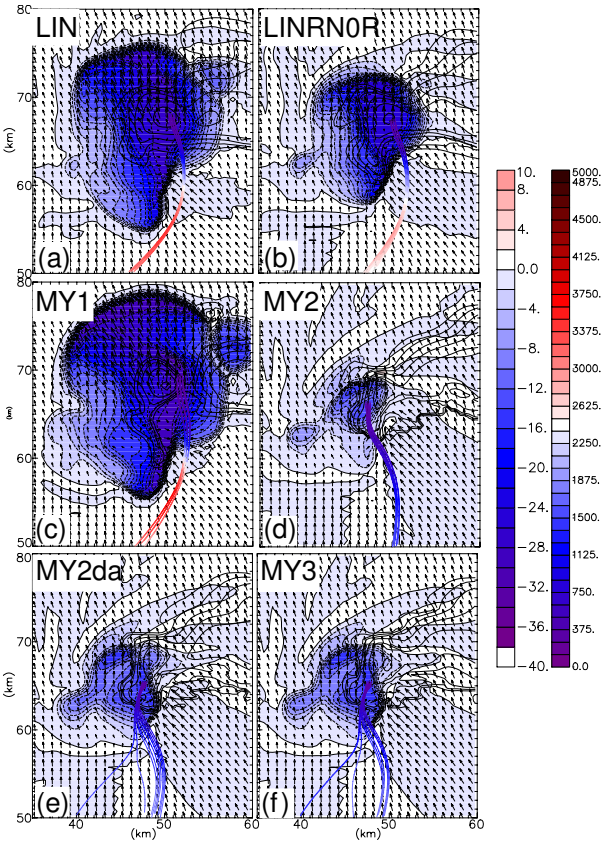

Fig. 6. Surface θ_e' (color fill), reflectivity (black contours, 10 dBZ increment), wind vectors every 1 km (1 unit = 7.5 m s^{-1}), and trajectories terminating in and near region of minimum θ_e' near the precipitation core.

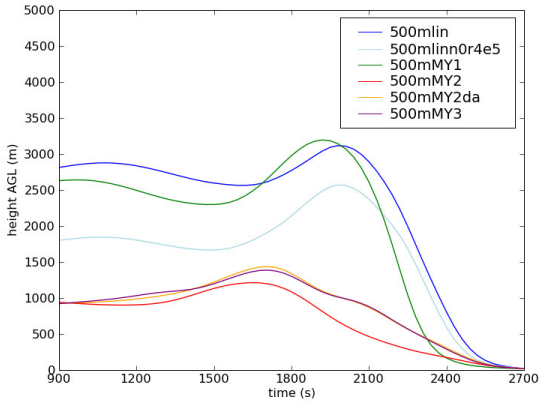

Fig. 7. Average heights vs. time for the trajectory groups in Fig. 6 for each of the simulations.

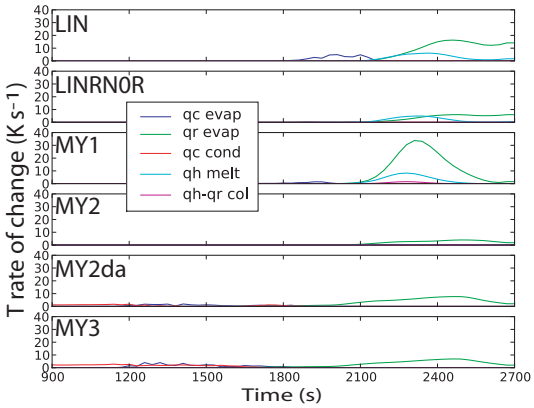

Fig. 8. Averaged instantaneous temperature rates due to microphysical processes along trajectories for each of the simulations.

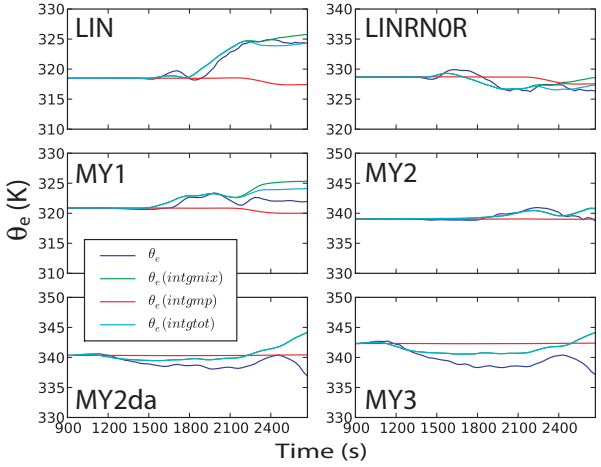

Fig. 9. θ_e vs. time (averaged) for each of the simulations. Shown are directly-interpolated values (blue), integrated values from mixing (green), integrated values due to microphysical processes (red), and combined (cyan).

Nevertheless, examining the general trend of the integrated θ_e is instructive, and the results shown here indicate that both turbulent mixing and microphysical processes are important in causing θ_e changes, and that θ_e tends to decrease along the trajectories in each run, due to melting of hail and turbulent mixing with surrounding parcels.

5. DISCUSSION

The results of this study strongly indicate that a significant improvement in various features of the simulated supercell storm occurs when moving from SM to DM microphysics. In the context of this study, a most interesting result is the dramatic reduction in cold pool intensity and size between the SM and DM (and higher) simulations. The budget and trajectory analyses indicate that both melting of hail and evaporation of rain are reduced in the MM simulations. We now turn to a discussion of the likely reasons for these large differences.

First, we discuss the well-known sensitivity of evaporation and melting to changes in the intercept parameter N_0. Considering only rain evaporation, for simplicity (arguments for hail melting are qualitatively similar), we note that the parameterization of bulk evaporation of rain used in the MY scheme is given by Eqn. (7) in MY05b. Noteworthy is the fact that, neglecting the ventilation term, the bulk rain evaporation rate is directly proportional to the intercept parameter N_{0r}. All other things being equal, a reduction in N_{0r} will produce a corresponding reduction in evaporation rate.

The dependence of evaporation rate on N_{0r} explains the strong sensitivity to cold pool intensity and size seen in previous studies with SM schemes that varied the value of N_{0r} for rain and/or hail. However, as has been found by observational studies and previous numerical simulations with DM microphysics (e.g., Waldvogel 1974, Ferrier et al. 1995), N_{0r} can vary in time and space, even within the same convective system. Thus, a fixed global value of N_{0r} may lead to large errors, even over the course of a simulation or prediction of a single case. As previously discussed, a DM scheme allows N_0 to vary independently and presumably consistently with the dynamical and microphysical processes ongoing in a given simulation. For a given precipitation event, N_0 may be on average larger, smaller, vary greatly, or vary slightly.

In the MY2 simulation, where the shape parameter α was fixed at 0 for all precipitating categories, corresponding to exponential distributions, it was shown that values of N_t were dramatically reduced in the downdrafts for both rain and hail for comparable or lesser magnitudes of mixing ratio than in the SM simulations, which is equivalent to shifting the particle size distribution (PSD) toward larger diameters, and correspondingly reducing N_0, for a given mixing ratio q, which in turn leads to lower evaporation or melting rates. For the MY2da and MY3 simulations, the physical meaning of N_0 changes, due to the dependence on α, which is allowed to vary over a wide range of positive values. It can be shown that an increase in α for a given fixed q and N_t actually enhances evaporation because, while the spectrum narrows and both the number of largest drops and the number of smallest drops decreases, the drops in the middle part of the spectrum increase such that the total surface area of the drops increases (Cohen and McCaul 2006).

MY05a found that size-sorting is one reason for the larger values of D_m (and thus smaller N_0 in the exponential MY2 case) in the low levels, due to the differential fall speeds of the number concentration and mixing ratio fields, the latter falling faster than the former. Physically, this translates to larger raindrops and hailstones fall faster than smaller ones. The larger particles evaporate or melt less efficiently, leading to

smaller magnitudes of evaporation and melting rates in the low-level downdrafts. In a SM scheme, however, a single fall speed is used for all particles in the distribution. For most SM schemes, including the ones herein, where mixing ratio is predicted, the mass-weighted mean terminal fall speed is used. This leads to the unphysical behavior of the very smallest particles falling too quickly, and the largest particles too slowly. Since the small particles are allowed to reach lower levels, this directly translates into larger, unphysical, evaporation rates in the low-levels.

In addition to the effect of size-sorting, for a SM scheme that fixes N_0, evaporation of a population of raindrops yields an increase in slope. This leads to yet another unphysical behavioral characteristic of these types of SM schemes. An increase in slope λ for an exponential distribution, while reducing q and holding N_0 constant, is physically equivalent to reducing the concentration of the largest drops from the distribution faster than the concentration of the drops at the small drop end of the spectrum mostly unaffected, a result opposite to that from physical intuition and theoretical studies of evaporation within rainshafts (e.g., Tzivion et al. 1989, Li and Srivastava 2001). It can be seen that evaporation in this case actually shifts the entire population of drops towards smaller diameters, leaving a considerable number of small to medium size drops still left to contribute to high evaporation rates, when in reality these drops would likely quickly be depleted (except for perhaps the very smallest drops; see previous references). We argue that these two unphysical effects taken together are at least partially responsible for the large evaporation rates and the attendant strong downdrafts and cold pools seen in many past and contemporary simulations of convective storms with SM schemes. However, SM schemes that do not hold N_0 fixed but rather other PSD-related parameters, such as the mean-mass diameter D_m (e.g. (van den Heever and Cotton 2004)) would not suffer from this particular issue, while the issue of sensitivity to choice of the fixed parameter still remains.

On the other hand, in the MM schemes used in this study, the slope (and thus D_m) is assumed to remain constant during the process of evaporation (but not melting of hail, where D_m decreases during the melting process). As such, evaporation would reduce both q and N_t at the same relative rate, leading to a corresponding reduction in N_0 for the exponential case. Physically, this translates to individual particles across the distribution being shifted down the spectrum towards smaller sizes as they evaporate, with the population as a whole maintaining the same mean mass. The smallest drops leave the distribution at the small end by being converted to vapor, a process much more physically reasonable than the SM case. This DM closure assumption for the rate of decrease of N_t is still not entirely correct since it implies that the mean-mass drop diameter does not change due evaporation, and thus overestimates the rate of decrease of N_t. Nevertheless, it is a distinct improvement over the fixed-N_0 assumption used in most SM schemes.

To test the above hypotheses regarding the effects of size-sorting and the differences between treatment of pure evaporation in the SM vs. MM case, we performed idealized 1D simulations of a distribution of rain drops falling in sub-saturated air, using all four versions of the MY scheme. To isolate these effects as cleanly as possible, the simulations were made as simple as possible, while still being physically reasonable. The following restrictions were applied: only the process of rain evaporation and sedimentation were modeled and no collision or breakup was allowed. The reader is referred to Feingold et al. (1991) for a discussion of the importance of these effects on evaporation. The atmosphere was assumed quiescent and isentropic with a base state potential temperature of 300 K, a surface pressure of 1000 hPa, and a constant saturation ratio of 0.6. No feedback from the evaporation of the falling rain to the atmosphere was allowed in either the temperature or moisture fields. Physically, this is equivalent to assuming that the rain is falling into a region where air is continually being replaced by sub-saturated air at a particular potential temperature. Since the convective downdrafts in this study were sub-saturated and were characterized by entrainment of dry mid-level environmental air, this is a reasonable assumption for the purposes of these tests.

At the top boundary, a M-P distribution of rain was specified as initial and boundary conditions for the falling rain field, with a constant intercept parameter of 8.0×10^6 m^{-4}. The vertical grid spacing was a uniform 100 m over a depth of 5 km, and a time step of 5 s was used. The results of the tests are summarized in Fig. 10. In addition to the four default simulations shown in Fig. 10a-d where both size-sorting and evaporation are active, Fig. 10e-g correspond to the MY2, MY2da, and MY3 schemes, respectively, with size-sorting turned off by setting the fall speeds for the N_t and Z fields equal to that of the q field. The vertical profiles all reached a steady state after approximately 30-45 min and thus the profiles at 45 min are shown for each case. As expected, the MY1 scheme shows the most evaporation over the greatest depth of any of the simulations, followed by the MY3, MY2da, and MY2 schemes in order of decreasing evaporation. The removal of size-sorting leads to stronger and deeper evaporation, though not as great as the MY1 case.

Thus, these results corroborate the argument that both size-sorting and the treatment of evaporation by fixing the slope parameter in the MM schemes leads to reduced evaporation of a falling rain shaft, and by extension, weaker, shallower downdrafts and weaker cold pools. It should be noted, that, in a more realistic scenario, the cooling by evaporation would tend to drive a downdraft, and thus, in the case of the MY1 column simulation (Fig. 10a), where most of the rain actually evaporates before reaching the ground, a strong convective downdraft would tend to lead to a downward displacement in the peak of the evaporation rate profile,

as well as leading to more *q* in low-levels. Similar arguments apply to the other schemes, but obviously dictated by the respective strengths of the diabatically-enhanced downdrafts.

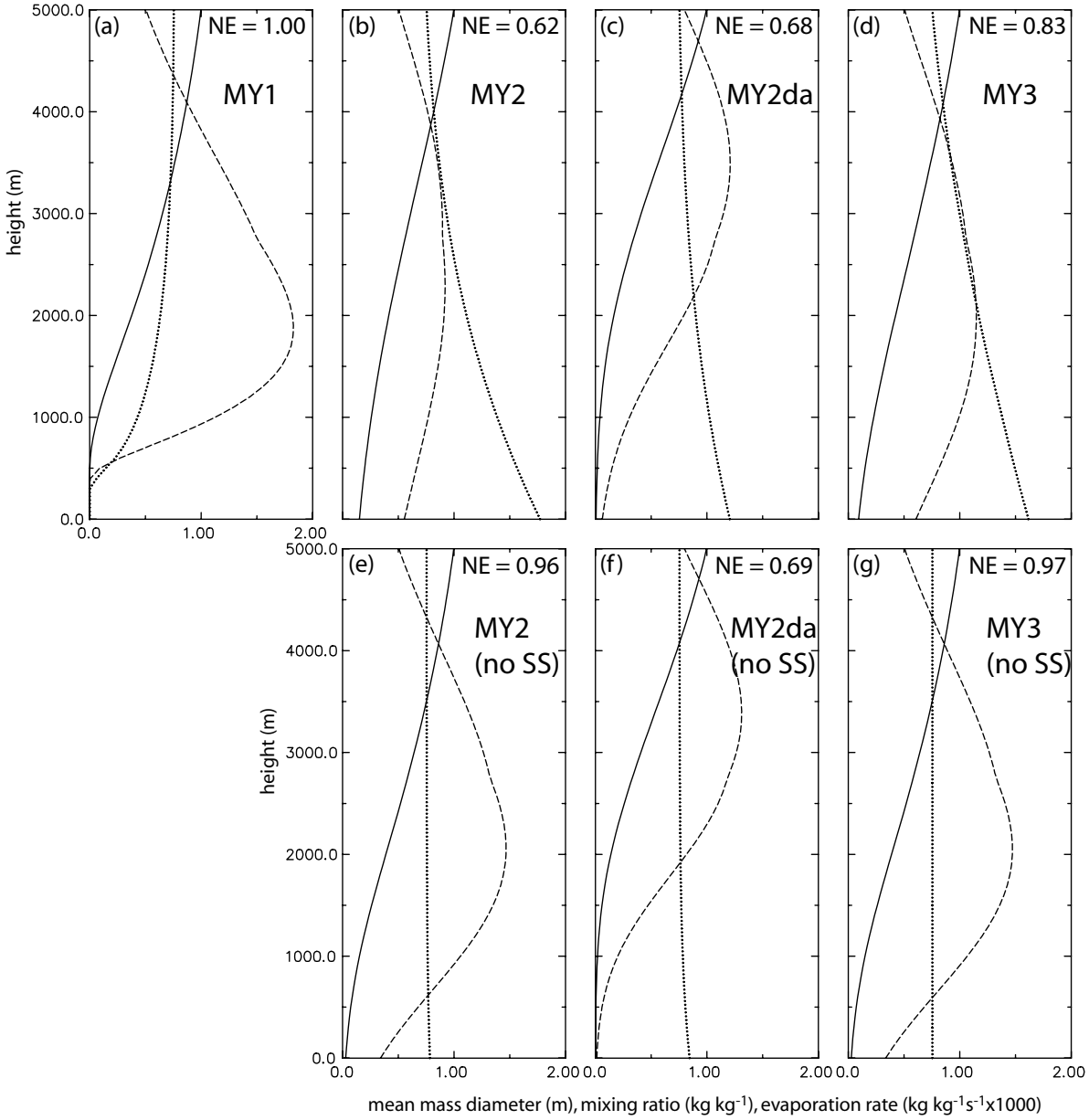

Fig. 10. Vertical profiles of rain mixing ratio q_r (kg kg^{-1}, solid), mean-mass diameter D_{mr} (m, dotted), and evaporation rate (kg kg^{-1}s^{-1}×1000, dashed) for the simple sedimentation-evaporation column model for a) MY1, b) MY2, c) MY2da, d) MY3, e) MY2 with no size-sorting, f) MY2da with no size sorting, and g) MY3 with no size sorting. Also shown in each panel is the normalized total evaporation (NE) over the previous 45 min relative to the MY1 scheme.

6. SUMMARY, CONCLUSIONS, AND FUTURE WORK

In this paper, we have analyzed high-resolution idealized simulations of the 3 May 1999 OK tornadic supercell thunderstorms. The goal of this study was to test the impact of a MM microphysics scheme on the development and evolution of the storms, and in particular the downdraft and cold pool properties. We found that the MM schemes, in general, performed better than their SM counterparts when typical fixed values of the intercept parameter N_0 were used in the SM schemes. The MM schemes showed overall weaker and moister cold pools, which is consistent with

available observations. In addition, the forward flank region was more developed and closer to the size and shape of the observed forward flank regions of the mature supercells on this day. This was attributed to the process of size-sorting of hydrometeors, which is parameterized in the MM schemes, but not in the SM schemes (MY05a).

We further demonstrated through the use of budget and trajectory analyses, that the MM schemes yield less water mass (both liquid and solid) in the low-level downdrafts, and larger average particle sizes, both of which lead to significantly lower amounts of evaporation and melting and associated diabatic cooling. While the FFD reaches the surface at times in the SM simulations, it remains elevated above the surface in the MM simulations, which is more consistent with the observations. In addition, the source region for air reaching the surface in the downdrafts comes from lower in the troposphere for the MM simulations than in the SM simulations, reflecting the higher θ_e in the cold pools of the MM storms.

Through an examination of the parameterized processes of evaporation and melting in the BMP's used in this study, we show that the MM schemes have a few important advantages over the SM schemes in their treatment of these processes, which relate mostly to how the size distribution is allowed to change more flexibly in the MM schemes. In particular, size-sorting of hydrometeors leads to a bias towards larger particles over smaller particles in the low-levels, leading to less evaporation and melting there. Also, the change in the PSD during evaporation or melting is handled in a more physically-consistent manner in the MM schemes by allowing N_0 to decrease during the evaporation process, while it is held fixed in the SM schemes. Results from a simplified column model that includes sedimentation and evaporation processes confirm a decreased evaporation magnitude for a steady-state rain shaft when using a MM scheme. Taken together, these two advantages, and possibly others that are not considered here, lead to a much better representation of evaporation and melting in the low-level downdrafts of the simulated supercell storms in this study.

In ongoing work, we are revisiting the real-data simulations with the smaller grid-spacings used in the idealized simulations in this study, to examine the robustness of these results under the more complicated scenario with an inhomogeneous environment in time and space, and where other diabatic physical processes such as radiation and surface friction are operating. Preliminary results suggest that, while the real-data MM simulations do not show as dramatic an improvement in cold pool structure as their idealized counterparts, nevertheless, there is significant improvement in the predicted track, reflectivity structure, and tornadic activity over the SM simulations. This is consistent with previous work which found extreme sensitivity of simulated tornadogenesis to changing parameters in a SM scheme (Snook and Xue 2006). Finally, in the future, we wish to make a more rigorous comparison of the results of the MM simulations of the hydrometeor fields in the supercells with observations, such as by comparing with polarimetric radar retrievals of hydrometeor fields.

Acknowledgement: This work was primarily supported by NSF grant ATM-0530814, the National Defense Science and Engineering Graduate Research Fellowship, and the National Science Foundation Graduate Fellowship, both awarded to the first author.

REFERENCES

Bolton, D., 1980: The computation of equivalent potential temperature. *Mon. Wea. Rev.*, **108,** 1046-1053.

Cohard, J.-M. and J.-P. Printy, 2000: A comprehensive two-moment warm microphysical bulk scheme. I: Description and tests. *Q. J. Roy. Meteor. Soc*, **126,** 1815-1842.

Cohen, C. and E. W. McCaul, 2006: The Sensitivity of Simulated Convective Storms to Variations in Prescribed Single-Moment Microphysics Parameters that Describe Particle Distributions, Sizes, and Numbers. *Mon. Wea. Rev.*, **134,** 2547-2565.

Dawson, D. T., II, M. Xue, J. A. Milbrandt, M. K. Yau, and G. Zhang, 2007: Impact of multi-moment microphysics and model resolution on predicted cold pool and reflectivity intensity and structures in the Oklahoma tornadic supercell storms of 3 May 1999. *22nd Conf. Wea. Anal. Forecasting/18th Conf. Num. Wea. Pred.*, Salt Lake City, Utah, Amer. Meteor. Soc., CDROM 10B.2.

Feingold, G., Z. Levin, and S. Tzivion, 1991: The evolution of raindrop spectra. Part III: Downdraft generation in an axisymmetrical rainshaft model. *J. Atmos. Sci.*, **48,** 315-330.

Ferrier, B. S., W. K. Tao, and J. Simpson, 1995: A double-moment multiple-phase four-class ice scheme. Part II: Simulations of convective storms in different large-scale environments and comparisons with other bulk parameterizations. *J. Atmos. Sci.*, **52,** 1001-1033.

Ferrier, B. S., W.-K. Tao, and J. Simpson, 1995: A double-moment multiple-phase four-class bulk ice scheme. Part II: Simulations of convective storms in different large-scale environments and comparisons with other bulk parameterizations. *J. Atmos. Sci.*, **52,** 1001-1033.

Gilmore, M. S., J. M. Straka, and E. N. Rasmussen, 2004: Precipitation uncertainty due to variations in precipitation particle parameters within a simple microphysics scheme. *Mon. Wea. Rev.*, **132,** 2610-2627.

Li, X. and R. C. Srivastava, 2001: An Analytical Solution for Raindrop Evaporation and Its Application to Radar Rainfall Measurements. *J. Appl. Meteor.*, **40,** 1607-1616.

Lin, Y.-L., R. D. Farley, and H. D. Orville, 1983: Bulk parameterization of the snow field in a cloud model. *J. Climate Appl. Meteor.*, **22,** 1065-1092.

Markowski, P. M., 2002: Mobile Mesonet Observations on 3 May 1999. *Wea. Forecasting*, **17,** 430–444.

Markowski, P. M., J. M. Straka, and E. N. Rasmussen, 2002: Direct surface thermodynamic observations within the rear-flank downdrafts of nontornadic and tornadic supercells. *Mon. Wea. Rev.*, **130,** 1692-1721.

Marshall, J. S. and W. M. Palmer, 1948: The distribution of raindrops with size. *J. Meteor.*, **5,** 165-166.

Meyers, M. P., R. L. Walko, J. R. Harrintong, and W. R. Cotton, 1997: New RAMS cloud microphysics parameterization. Part II: The two-moment scheme. *Atmos. Res.*, **45,** 3-39.

Milbrandt, J. A. and M. K. Yau, 2005: A multi-moment bulk microphysics parameterization. Part II: A proposed three-moment closure and scheme description. *J. Atmos. Sci.*, **62,** 3065-3081.

——, 2005: A multi-moment bulk microphysics parameterization. Part I: Aanlysis of the role of the spectral shape parameter. *J. Atmos. Sci.*, **62,** 3051-3064.

Reisner, J., R. M. Rasmussen, and R. T. Bruintjes, 1998: Explicit forecasting of supercooled liquid water in winter storms using the MM5 mesoscale model. *Quart. J. Roy. Meteor. Soc.*, **124,** 1071–1107.

Seifert, A. and K. D. Beheng, 2006: A two-moment cloud microphysics parameterization for mixed-phase clouds. Part 1: Model description. *Meteorology and Atmospheric Physics*, **92,** 45-66.

Snook, N. and M. Xue, 2006: Sensitivity of supercell tornado simulations to variations in microphysical parameters. *Preprint, Fourth Joint Korea-U.S. Workshop on Mesoscale Observation, Data Assimilation and Modeling for Severe Weather*, Soul, Korea.

Straka, J. M. and J. R. Anderson, 1993: The numerical simulations of microburst producing thunderstorms: Some results from storms observed during the COHMEX experiment. *J. Atmos. Sci.*, **50,** 1329-1348.

Tao, W.-K. and J. Simpson, 1993: Goddard cumulus ensemble model. Part I: Model description. *Terres. Atmos. Ocean Sci.*, **4,** 35-72.

Tzivion, S., G. Feingold, and Z. Levin, 1989: The Evolution of Raindrop Spectra. Part II: Collisional Collection/Breakup and Evaporation in a Rainshaft. *J. Atmos. Sci.*, **46,** 3312-3328.

van den Heever, S. C. and W. R. Cotton, 2004: The Impact of Hail Size on Simulated Supercell Storms. *J. Atmos. Sci.*, **61,** 1596-1609.

Waldvogel, A., 1974: The N0-jump of raindrop spectra. *J. Atmos. Sci.*, **31,** 1067-1078.

Xue, M., D.-H. Wang, J.-D. Gao, K. Brewster, and K. K. Droegemeier, 2003: The Advanced Regional Prediction System (ARPS), storm-scale numerical weather prediction and data assimilation. *Meteor. Atmos. Physics*, **82,** 139-170.

Xue, M., K. K. Droegemeier, V. Wong, A. Shapiro, K. Brewster, F. Carr, D. Weber, Y. Liu, and D. Wang, 2001: The Advanced Regional Prediction System (ARPS) - A multi-scale nonhydrostatic atmospheric simulation and prediction tool. Part II: Model physics and applications. *Meteor. Atmos. Phys.*, **76,** 143-166.

Ziegler, C. L., 1985: Retrieval of thermal and microphysical variables in observed convective storms. Part I: Model development and preliminary testing. *J. Atmos. Sci.*, **42,** 1487-1509.